APPLICATION OF PIV TECHNIQUE FOR THE STUDY OF CAVITATING FLOWS ABOUT A CASCADE OF 2D HYDROFOILS

A.YU. KRAVTSOVA[1,2], D.M. MARKOVICH[1,2,c], K.S. PERVUNIN[1,2], M.V. TIMOSHEVSKIY[1,2]

[1]Institute of Thermophysics SB RAS, Novosibirsk, 630090, Russia
[2]Novosibirsk State University, Novosibirsk, 630090, Russia

[c]Corresponding author: Tel/Fax: +73833309040; Email: dmark@itp.nsc.ru

KEYWORDS:

Main subjects: turbulent structure, cascade of hydrofoils
Fluid: steady and unsteady cavitating flows, partial cavities
Visualization method(s): Particle Image Velocimetry, high-speed photography
Other keywords: NACA0015, cavitation cloud shedding, flow separation

ABSTRACT

The main emphasis of the work is put on experimental study of spatial structure and dynamics of gas-vapor cavities and turbulent structure of cavitating turbulent flows around a single NACA0015 hydrofoil and a cascade of three identical NACA0015 hydrofoils. The flows were investigated for different angles of incidence α = 0, 3, 6 and 9º with variation of cavitation number σ from 6 for the cascade down to 0.6 for the single hydrofoil. As a result, the full set of statistical moments of turbulent fluctuations (including the third-order ones) was calculated for all regimes. Comparison of turbulent characteristics was performed for different cavity types and the main peculiarities of the flows were pointed out.

INTRODUCTION

The problems relating to cavitation and erosion caused by cavitation belong to the most complex fundamental challenges of modern hydrodynamics. The most important requirements for safe and efficient operation of hydropower systems are reliability and longevity of the equipment used. As a rule, operation of real power systems, such as hydroturbines, and hydrotechnical equipment constructions, e.g. supply ducts and draft tubes of hydropower plants, are accompanied, in practice, by unsteady turbulent flows of complex geometry that are often two-phase. A rise of operation time and material endurance, increase of hydromachinery efficiency and degree of its safety are impossible without studying physical mechanisms of hydrodynamic processes, where large-scale vortices (LSV) and cavitation play the key role. Interaction of LSV with gas-vapor dispersed phase is a complex non-linear process strongly influencing cavitation erosion on hydraulic units and pulsation characteristics of the flows due to mutual impact of continuous and dispersed phases. Trajectories of dispersed phase particles (bubbles) can be affected by local non-equilibrium turbulence in liquid (turbulent dispersion), while the bubbles motion significantly changes properties of turbulent fluctuations in the carrier phase (turbulence modulation) due to a number of physical mechanisms. As known, the occurrence of resonance effects can lead to excessive vibration loads and, as a consequence, failure of hydraulic equipment or, at worst, even emergencies. Thus, it becomes obvious that simultaneous investigation of dynamics of partial cavities and LSV developing in shear-layers and study of interaction of LSV with gas-vapor dispersed phase in unsteady turbulent two-phase flows are rather important problems from the standpoint of fundamental science and applied research (e.g. in the field of improvement of modern hydrotechnical equipment constructions). In order to forecast cavitation erosion and have an ability to control cavitation, the detailed experimental data on turbulent structure of flows, i.e. spatial distributions of instantaneous velocity, vorticity and pressure fields and turbulent characteristics, is of a high interest. It should be also noted that developed and suggested methods on reducing the negative effects of cavitation have to satisfy the requirement of power loss minimization. This can be implemented only if the profound knowledge about the hydrodynamic processes occurring in hydroturbine settings is available.

Presently, one can find a number of papers in literature that are devoted to experimental modeling of cavitating flows around 2D hydrofoils. However, experimental results obtained in works by different authors often diverge.

Generally, the main results represent visual observations and regime maps with qualitative descriptions, point pressure measurements and sometimes the velocity distributions in the region free of cavitation bubbles. In some works, effects of local volume fraction of vapor phase within cavity and in a wake past a foil, liquid temperature, etc., on spatial structure and dynamics of partial cavities were also studied. Depending on flow conditions (hydrofoil surface shape, velocity and pressure fields, at alias), one can distinguish a variety of cavitation patterns (bubble, vortex, cloud and supercavitation, etc.). All types of gas-vapor cavities are divided into partial and super cavities. Partial cavities occur when a cavity closes on the cavitating surface, while a super cavity closes downstream in the wake of the cavitating object. Partial cavitation has further classification (see Laberteaux and Ceccio (2001) 10 for more details). In that work, the authors showed the essential influence of adverse pressure gradients on formation of a turbulent wake. With this, cloud cavitation arises when a large portion of cavity filled with re-entrant fluid breaks off, forming a cavitation cloud. Cervone et al. (2006) 1 studied the impact of thermal cavitation effects on the onset of various forms of cavitation and instabilities. As a result, cavitation regimes were divided into three different zones, which correspond to different behaviours of the upstream pressure frequency spectrum.

When a sheet cavity reaches a certain dimension, periodic oscillations of cavity appear, this process is accompanied by cavity (in the form of clouds) shedding downstream. In the paper by Kubota et al. (1989) 9, the authors showed that the cloud cavity consists of a large-scale vortex and cluster of a bulk of small vapor bubbles situated in the centre of the vortex, using Laser Doppler Anemometry approach together with conditional sampling method. In various experiments (e.g. George et al. (2000) 7), it was revealed that oscillations of the cloud cavities have very close Strouhal numbers. Further studies proved a correlation between cloud cavitation and re-entrant jet generated in the region of the cavity closure as a result of the action of opposite pressure gradient (see Callenaere et al. (2001) 4 and Kawanami et al. (1997) 8).

Nevertheless, in spite of a large amount of works on investigation of cavitating flows, detailed quantitative information required for optimisation and verification of existing mathematical models is still extremely restricted even for simplified conditions. This is because of difficulty or even impossibility of performing experiments under the full-scale conditions and high costs of tests at expensive laboratory setups. Due to the complexity of cavitating turbulent flows, comprehensive experimental information on the hydrodynamic structure of such flows is extremely useful from the standpoint of development and verification of modern numerical approaches for simulation of sufficiently anisotropic turbulent multi-phase flows. In terms of elaboration of mathematical models describing inception and development of cavitation, the main interest is focused on complex experimental investigations under the simplified geometric conditions (Venturi nozzles, scaled-down shaped bodies, e.g. NACA series hydrofoils, etc.). Acquisition of systematic experimental data for various cavitation regimes is a crucial problem.

EXPERIMENTAL SETUP

Experiments were carried out at the Cavitation tunnel of the Institute of Thermophysics SB RAS, which represents a closed hydrodynamic circuit. The setup is equipped with two centrifugal pumps, ultrasonic flowmeter, temperature and pressure sensors (see Fig. 1). Dimensions of the tunnel are as follows (LxHxW): 8.4x2.2x1.1 m. Its working section consists of heat exchanger, honeycomb, confuser, test section and diffuser. The temperature of the working liquid is maintained constant by means of the temperature control system consisting of the temperature sensor and electromagnetic valve driven by a PID control. The honeycomb cells are of 25×25 mm cross-section and 500 mm length. The confuser of 790 mm length is made by the fourth-power polynomial profile; the degree of flow compression is equal to 16. The test section is a channel of 80×250 mm rectangular cross-section and 1.3 m length with flat parallel sidewalls. The sidewalls of the test section are equipped with transparent windows to perform visual observations. The divergence angle of diffuser sidewalls adjoining the smaller sidewalls of the test section is 3.5°, while those abutting upon the larger sidewalls are parallel. A special shaft is located above the heat exchanger in order to regulate the static pressure inside the circuit. The reverse channel of the setup includes a swivel elbow on 180 degrees with 750 mm radius and 250x250 mm cross-section, straight pipeline of 300 mm diameter, flow-measuring part and duct supplying working liquid to the pumps. The maximum flow rate through the contour is 1100 m^3/h, what corresponds to the maximum free flow velocity of 15.3 m/s. The flow rate is adjusted by changing rotation speed of the pumps by frequency convertors.

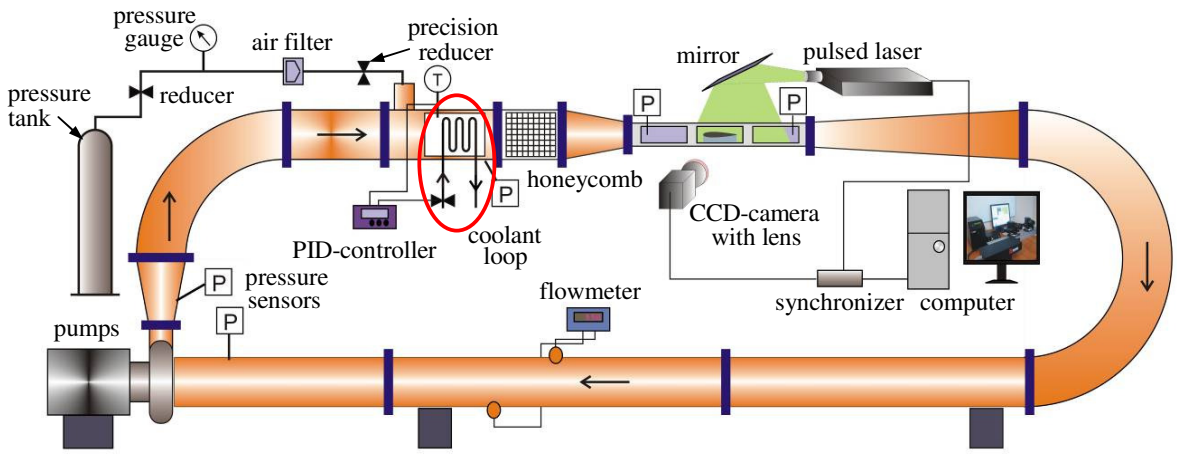

Fig. 1 Sketch of Cavitation tunnel at Institute of Thermophysics SB RAS: P, T – pressure and temperature transducers.

EXPERIMENTAL CONDITIONS AND MEASUREMENT TECHNIQUE

In the work, dynamics and spatial structure of partial cavities as well as turbulent characteristics of the flows about a NACA0015 series hydrofoil (100 mm chord) and a cascade of three NACA0015 hydrofoils were investigated in detail for four attack angles α = 0, 3, 6 and 9°. In case with the cascade, the distance between adjacent foils was 60 mm. In order to have optical access to the central foil of the cascade, which is the most representative from the standpoint of modeling, the upper foil was made of polished plexiglass. The other bodies were of brass with relatively high level of roughness (about 2.5 μm).

The working liquid was distilled water. The water was not deaerated, the amount of dissolved air in liquid was estimated by Henry's law under the normal conditions and it equaled approximately 0.023 g of air in 1 kg of water. The liquid temperature was equal to 30°C. Overpressure in the setup was fixed and set at 59 kPa. In order to achieve different conditions nearby the bodies and, consequently, to observe various cavity patterns, cavitation number, $\sigma = (P_{in} - P_{vap})/(\rho \cdot U_0^2/2)$, defined as difference of static pressure at the inlet part of test section, P_{in}, and water vapor pressure, P_v, divided by flow strength was varied in the range from 0.6 to 6 in experiments by changing the mean flow velocity. Under the present conditions, P_v = 0.044 bar. The initial level of turbulent fluctuations in the flow, u_{rms}/U_0, was lower than 1%. The Reynolds number, Re, based on mean flow velocity, U_0, and chord length, L, lied in the range from 1×10^6 to 2×10^6. The Strouhal number, Sh = $f \cdot C/U_0$, determined as the ratio of product of maximal cavity length, C, and characteristic frequency of cloud cavity shedding, f, to mean flow velocity, U_0, for the current regime was about 0.18 for the NACA0015 hydrofoil.

In order to analyze dynamics and spatial structure of gas-vapor cavities, high-speed visualization was carried out by means of Photron FASTCAM SA5 camera at the frame rate of 10 kHz from two positions: horizontal and vertical.

Velocity fields were measured by using PIV-system "POLIS" consisting of a double-pulsed Nd:YAG Quantel Big Sky EVG00200 laser (wavelength 532 nm, repetition rate 15 Hz, pulse duration 10 ns, pulse energy 200 mJ), CCD-camera (pixel depth 10 bits, matrix resolution 2048×2048 pixels) equipped with AF Nikkor 28 mm f/2.8D lens and optical low-pass filter (bandpass edge 570 nm), as well as synchronizing processor. The PIV-system was operated via a computer with "ActualFlow" software. The thickness of laser light sheet formed by a cylindrical lens to illuminate tracer particles was about 0.8 mm in the measurement plane that coincided with the middle longitudinal plane of the test section parallel to its larger sidewalls. The distance between the camera and the laser sheet was about 610 mm. The size of the measurement area was about 285×250 mm. In order to perform PIV-measurements correctly in cavitating flows, the fluorescent tracers (average size of 10 μm, wavelength range of 550–700 nm) were added into the working liquid.

The velocity fields were calculated, using the iterative cross-correlation algorithm with continuous window shift and deformation, 50% overlap of interrogation windows was applied as well. Sub-pixel interpolation of a cross-correlation peak was performed over three points, using one-dimensional approximation by the Gaussian function. In order to have relatively large dynamic range, the initial size of interrogation window was chosen to be 64×64 pixels. The size of the final interrogation window was 32×32 pixels in order to have relatively low level of noise. Inaccuracy of the offset determination did not exceed 0.1 pixels. Thus, the velocity measurement errors were 1% and 4% for tracer

offsets of 8 and 2 pixels, respectively. Obtained instantaneous velocity vector fields were validated with two procedures applied successively: Peak Validation with threshold 2.0 and Adaptive 7x7 Median Filter.

RESULTS AND DISCUSSION

All the results below are given only for $\alpha = 3°$. This value of the attack angle was selected as the most demonstrative for qualitative and quantitative description of characteristic features of cavitating flows. In all fields of turbulent characteristics, the reference point coincides with the leading edge of the hydrofoil in the measurement plane at $\alpha = 0°$.

In Fig. 2, typical cavity patterns on the cascade are presented for various regimes. As seen, cavitation initially occurs on the suction side of the boundary (upper for the case of positive α) hydrofoil. When cavitation number is about $\sigma = 1.54$, cavitation appears in the form of transitional cavity[1] (see Fig. 2-a), the two other foils being free of cavitation. This is caused by the wall effect. Wall vicinity leads to flow acceleration in the channel above the upper foil and, consequently, local pressure drop, which, in turn, results in cavitation inception under certain conditions. When cavitation number decreases, cavity on the upper hydrofoil grows and transition to cloud cavitation[2] occurs (e.g. see Fig. 2-b). In addition, transitional cavity on the central foil and sheet cavity[3] on the lower one arise when $\sigma = 1.4$. However, unlike the classical concept of cloud cavitation, in the present case the whole cavity separation from the foil surface was not detected. Instead of this, only relatively small separate clouds detached from the foil surface in the rear (frothy) half of the entire cloud cavity. It must be related to that the cavity is very thin, and therefore re-entrant jet flow cannot form completely. Subsequently, these small clouds were convected downstream by the main flow and collapsed rapidly because of static pressure growth. Vortex core cavitation was also observed behind the trailing edge of the hydrofoil. As it can be distinctly observed in Fig. 2-b, the leading edges of the cavities are located in the following way: the upper one – right behind the leading edge of the foil, the central and lower ones – at distances of $0.05L$ and $0.12L$ downstream from the leading edges of the corresponding foils. This is likely to be connected with vertical pressure gradient that is created by the foils mounted at non-zero incidence angle. Since cloud cavities are of quasi-periodical nature, pulsations of the cloud cavity closure on the upper foil produce those of the transitional and sheet cavities (Sh = 0.15), though the transitional and sheet cavities are relatively stable in case of a single hydrofoil. This occurs due to variation of pressure field in the whole flow imposed by cloud cavitation quasi-periodic behaviour. With further reduction in cavitation number (see Fig. 2-c), the cavities on all the foils continue to rise so that, when $\sigma = 1.3$, they all turn into cloud cavities (Sh = 0.14).

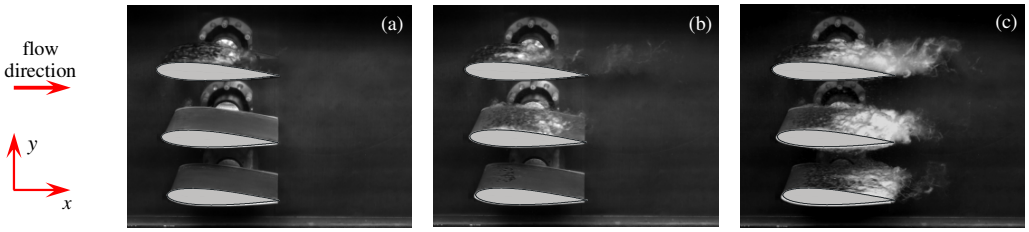

Fig. 2 Instantaneous images of partial cavities occurring on the cascade for (a) $\sigma = 1.54$ ($\xi = 1.13$), (b) $\sigma = 1.4$ ($\xi = 1.01$), (c) $\sigma = 1.3$ ($\xi = 0.94$). Angle between camera line-of-sight and horizontal line is 25°.

Development of the cavities during one period of cavity extent pulsations is demonstrated in Fig. 3 and 4 for two regimes. For $\sigma = 1.4$, dynamics of cavity length is as follows. First, the upper cavity rises up to its maximum length of about L, then its growth stops for a while and, simultaneously, the central and lower cavities start to rise until they reach their maximum extent about $0.7L$ and $0.34L$, respectively. After that, the rear half of the upper cavity spontaneously

[1] This cavity type is intermediate between sheet and cloud cavities. In general, at the closure region transitional cavity is accompanied by continuous shedding of small clouds and larger horseshoe-shaped ones consisting of a bulk of gas-vapor micro-bubbles.

[2] As widely acknowledged, cloud cavities are characterized by detachment of the whole cavity from foil surface and quasi-periodic cloud shedding process due to the appearance of re-entrant jet. For instance, detailed description of cloud cavitation can be found in Callenaere et al. (2001) [4].

[3] Sheet cavity represents a gas-vapor film of relatively stable length with clear interface. In the region of sheet cavity closure, main flow re-attaches to solid surface of a cavitating object.

begins to break off (this process is described above) and the upper cavity length decreases down to 0.5*L*. Thereafter, the central and lower cavities diminish. The minimum length of the central cavity is 0.3*L*, but the lower one disappears totally. Afterwards, this process repeats. For σ = 1.3, the cavity dynamics changes. All the cavities grow simultaneously until they achieve the lengths of 0.85*L*, 0.7*L* and 0.6*L*, respectively. Then only the upper cavity continues to rise to reach the trailing edge of the foil. After that, the central and lower cavities overtake the upper one and achieve the trailing edges of the corresponding foils as well. At this moment, free traveling bubble cavitation arises in the channels between the foils and above the upper hydrofoil. Cavities on the pressure sides of the upper and central foils were also registered. Thereafter, the upper cavity diminishes down to 0.5*L* and, later, the two other cavities start to collapse until they quite disappear. Usually the central cavity disappears later than the lower one, but sometimes it happens inversely. After this moment, the upper cavity extent decreases down to 0.25*L*. Afterwards, this process repeats.

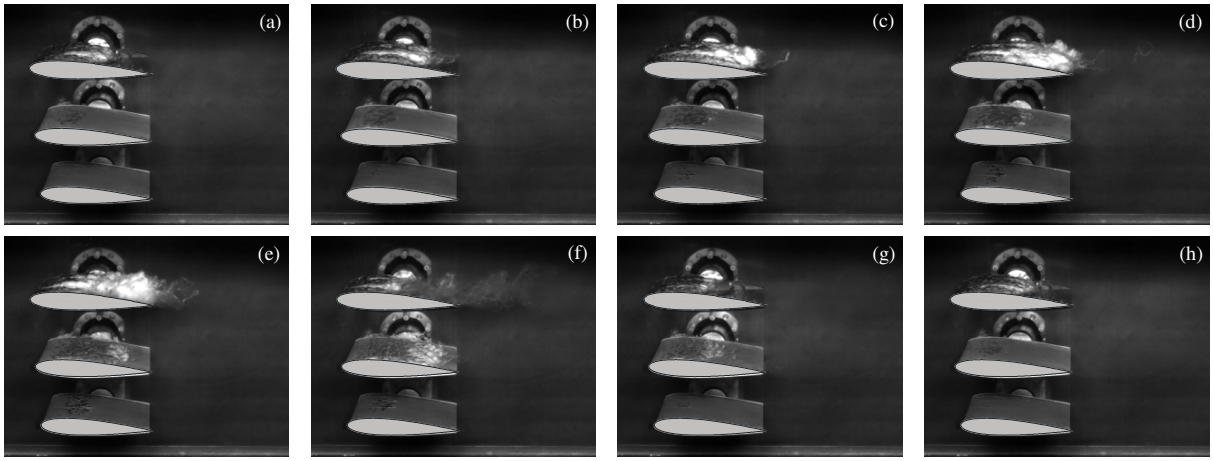

Fig. 3 Temporal evolution of the cavities within one cycle of quasi-periodical process of cavity extent pulsations for σ = 1.4 (Sh = 0.15). Time delay is 8.4 ms.

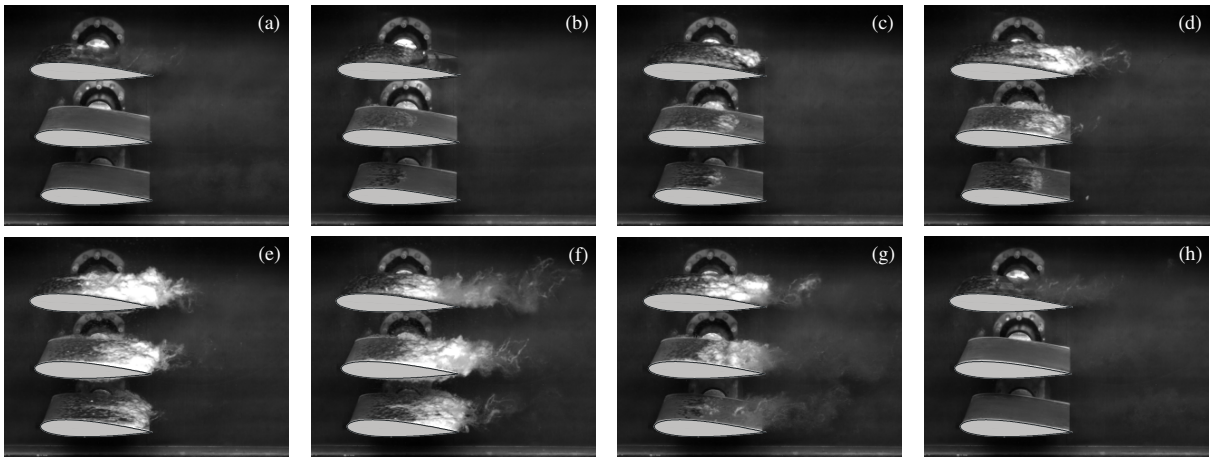

Fig. 4 Temporal evolution of the cavities within one cycle of quasi-periodical process of cavity extent pulsations for σ = 1.3 (Sh = 0.14). Time delay is 9.9 ms.

Basing on the ensemble of 5000 instantaneous velocity fields, 2D distributions of the mean velocity (see Fig. 5 and 6), turbulent kinetic energy (see Fig. 7 and 8) and third-order statistical moments of turbulent fluctuations (see Fig. 9 and 10) were calculated. Because of the laser sheet spread from the top along the symmetry plane of test section, the flow area below the foils was shadowed and, therefore, is masked grey in the figures. The flow direction is to the right.

In Fig. 5 and 6, one can observe that, in front of the leading edge, the flow locally decelerates and the region of slowdown shifts to the pressure side of the foils in all the cases. The minimum values of mean velocity in cross-section x/L = 0 are almost identical for all the regimes and equal to $U_{min}/U_0 \approx 0.73$ for the NACA0015 hydrofoil and 0.83 for

the center foil of the cascade. In a region above the upper side of the foils, mean velocity becomes higher than the mean flow velocity. When σ decreases, maximum of the mean velocity becomes slightly lower and shifts gradually downstream: from $U_{max}/U_0 \approx 1.35$ at point ($x/L = 0.2$; $y/L = 0.12$) for $\sigma = 1.36$ to $U_{max}/U_0 \approx 1.33$ at point ($x/L = 0.38$; $y/L = 0.12$) for $\sigma = 0.97$ in case with the NACA0015 foil and from $U_{max}/U_0 \approx 1.45$ at point ($x/L = 0.23$; $y/L = 0.07$) for $\sigma = 1.73$ to $U_{max}/U_0 \approx 1.44$ at point ($x/L = 0.38$; $y/L = 0.09$) for $\sigma = 1.3$ in case with the central foil of the cascade. This fact can be explained in the following way. As known, decrease in cavitation number results as in transition to another cavity type so, for a current cavity type, extension of the cavity and growth of cavity clouds that separate from the cavity and are involved downstream by the main flow. This behaviour is accompanied by pulsations of the cavity at its closure. Consequently, pulsations at the cavity trailing edge lead to increase of liquid velocity fluctuations (see Fig. 7 and 8) and, finally, to the reduction of the mean velocity values in this region.

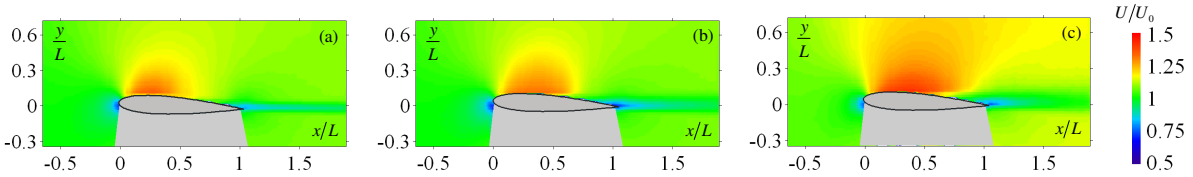

Fig. 5 2D distributions of longitudinal (x-direction) component of the mean velocity about the NACA0015 foil: (a) $\sigma = 1.22$, $C/L = 0.5$, (b) $\sigma = 1.05$, $C/L = 1$, (c) $\sigma = 0.97$, $C/L = 1.1$, Sh = 0.18.

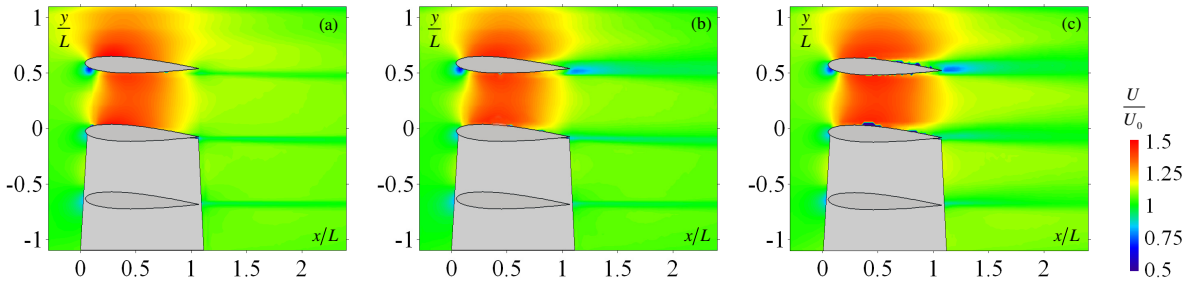

Fig. 6 2D distributions of longitudinal (x-direction) component of the mean velocity about the cascade: (a) $\sigma = 1.54$ ($\xi = 1.13$), (b) $\sigma = 1.4$ ($\xi = 1$), (c) $\sigma = 1.3$ ($\xi = 0.94$).

Downstream from the region of higher values of mean velocity along the suction side of the hydrofoil, the mean velocity drops below the values of mean flow velocity. For the NACA0015 hydrofoil, this takes place only at the trailing edge of the foil in the wake (see Fig. 5-a). The appearance of a region of lower values behind the body is directly connected to the flow separation from the foil surface and flow turbulization. As σ diminishes, the point of flow separation at the suction side slightly moves upstream and transverse extension of the turbulent wake also rises up to $0.14L$ for the cloud cavitation (see Fig. 5-c). Here it should be noted that this behaviour is averaged, i.e., at a certain moment, flow detachment from the surface occurs in some region (its extensions depend on the cavity type) around the separation point in the mean velocity fields.

Comparing the flow characteristics around the single NACA0015 hydrofoil and cascade, one can state that values of cavitation number strongly disagree for relatively neighboring regimes with close cavity lengths. This results in high complication of direct comparison of the flows. It is likely that classical definition of cavitation number (see nomenclature below) reproduces incorrectly the conditions of cavitation inception for the cascade. Therefore, to compare these two cases, a new quantity – local cavitation number – was introduced for the case with the cascade, which takes into consideration local conditions near the hydrofoils of the cascade, i.e. $\xi = (P - P_{vap})/(\rho \cdot U^2/2)$, where P and U are local values of mean static pressure and the longitudinal component of mean velocity, respectively. These values can be estimated, for example, at the middle line of foil passage in cross-section $x/L = 0$[4]. Using the present definition of local cavitation number, its values become quite close to those of cavitation number in case with the single hydrofoil (cf. Fig. 5 and 6).

[4] In the work, local values of mean static pressure was not measured but was estimated from Bernoulli equation, which can be applied to the flow region where liquid velocity fluctuations are small enough.

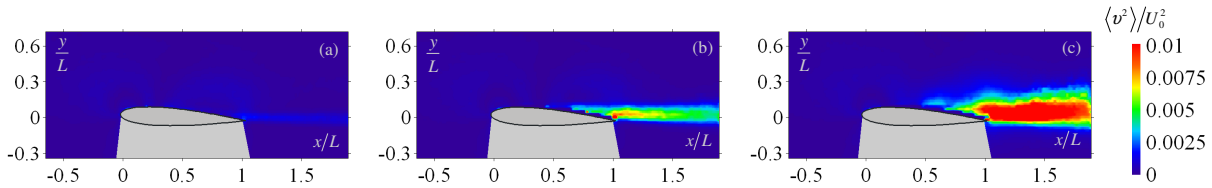

Fig. 7 2D distributions of transversal (y-direction) component of TKE about the NACA0015 foil: (a) $\sigma = 1.22$, $C/L = 0.5$, (b) $\sigma = 1.05$, $C/L = 1$, (c) $\sigma = 0.97$, $C/L = 1.1$, Sh = 0.18.

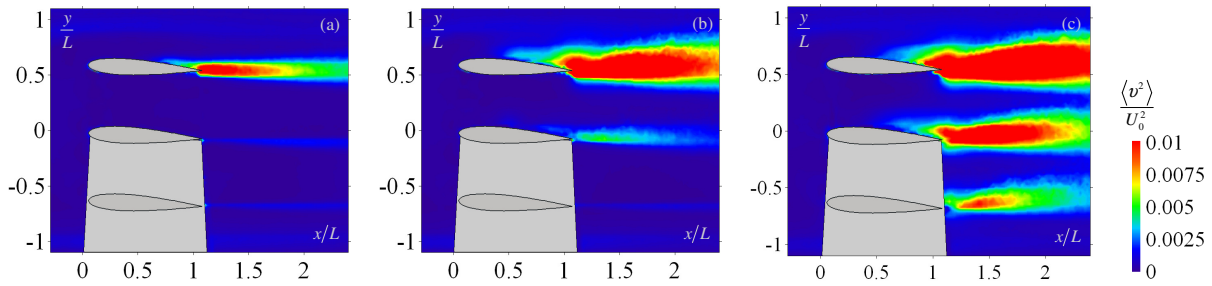

Fig. 8 2D distributions of transversal (y-direction) component of TKE about the cascade: (a) $\sigma = 1.54$ ($\xi = 1.13$), (b) $\sigma = 1.4$ ($\xi = 1$), (c) $\sigma = 1.3$ ($\xi = 0.94$).

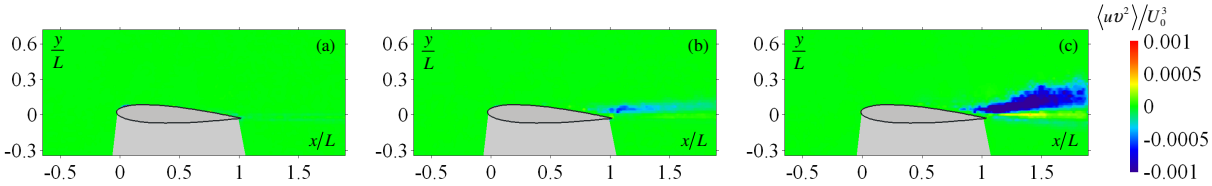

Fig. 9 2D distributions of the third-order moment of liquid velocity fluctuations about the NACA0015 foil: (a) $\sigma = 1.22$, $C/L = 0.5$, (b) $\sigma = 1.05$, $C/L = 1$, (c) $\sigma = 0.97$, $C/L = 1.1$, Sh = 0.18.

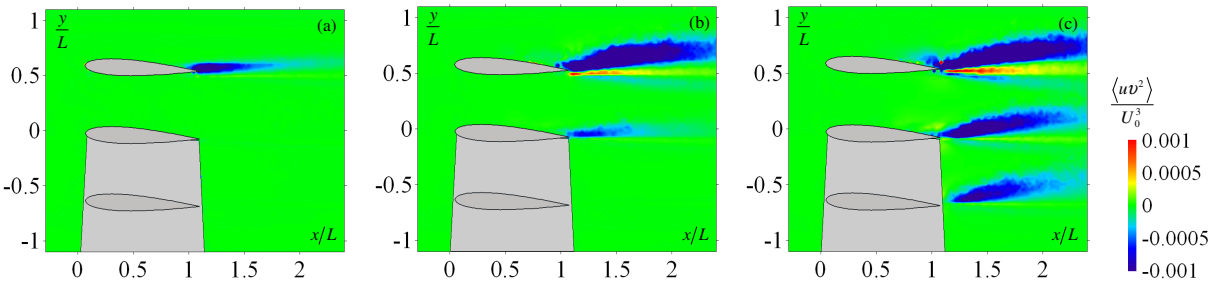

Fig. 10 2D distributions of the third-order moment of liquid velocity fluctuations about the cascade: (a) $\sigma = 1.54$ ($\xi = 1.13$), (b) $\sigma = 1.4$ ($\xi = 1$), (c) $\sigma = 1.3$ ($\xi = 0.94$).

Analyzing distributions of the transversal component of turbulent kinetic energy (TKE) in Fig. 7 and 8, the fields for the single foil and the cascade show that turbulent wakes behind the central foil in the cascade and the single foil are quite similar for all regimes. In whole, cavitation number decrease leads to the growth of liquid velocity fluctuations: at the trailing edge of the single foil, $\max(\langle v^2\rangle/U_0^2) \approx 0.002$ at point ($x/L = 1.02$; $y/L = 0.02$) for $\sigma = 1.36$ and $\max(\langle v^2\rangle/U_0^2) \approx 0.02$ at point ($x/L = 1.2$; $y/L = 0.02$) for $\sigma = 0.97$; behind the central foil of the cascade, $\max(\langle v^2\rangle/U_0^2) \approx 0.002$ at point ($x/L = 1.66$; $y/L = -0.08$) for $\sigma = 1.73$ and $\max(\langle v^2\rangle/U_0^2) \approx 0.023$ at point ($x/L = 1.23$; $y/L = -0.06$) for $\sigma = 1.3$. Thus, comparing the fields in Fig. 7 and 8, one can conclude that transition to cloud cavitation leads to global modification of the turbulent structure of the flow. As seen, $\langle v^2\rangle$ increases about 10 times for the case with the NACA0015 hydrofoil, however, the point where the maximum value of velocity fluctuations is reached moves downstream for the single foil and upstream for the cascade when transition to cloud cavitation occurs.

In Fig. 9 and 10, the fields of the third-order moment of velocity fluctuations corresponding to transfer of transversal component of TKE in the longitudinal direction due to turbulence itself (turbulent diffusion) are presented. This quantity is quite useful for closure of modern numerical approaches for cavitating flows modelling.

CONCLUSION

In the present work, 2D distributions of turbulent characteristics of the flows about the single NACA0015 hydrofoil and the cascade of three hydrofoils were measured including third-order moments by means of PIV/LIF technique. The measurements were performed for different regimes, starting from cavitation inception and finishing the cloud cavity.

High-speed visualization allowed to investigate qualitatively the dynamics and spatial structures of the cavities occurring on the cascade. When transition to cloud cavitation occurs, the hydrodynamic structure of the entire flow undergoes significant changes as compared to the cavitation-inception case. In the mean, progressive growth of gas-vapor cavity results in gradual shift of the flow separation point upstream. The cloud cavity leads to formation of an intense turbulent wake behind the cavity closure region, significant increase in its transverse extent, as well as intensification of turbulent fluctuations (about 3 times) due to generation of large-scale vortex structures in the shear layer over the vapor cavity.

In general, the work shows that, due to nonlinear nature of turbulent flows, cloud cavitation substantially changes the global pattern of the flow around the hydrofoil. With this, it becomes obvious that modern numerical simulation approaches should take into account these features of turbulent cavitating flows. For more complete analysis of the flow structure, it is obviously necessary to measure simultaneously the velocity of both phases as well as the concentration of the gas-vapor phase. Such a study will be possible by using modern sophisticated imaging techniques (one of them is PFBI, for more detailed description see Akhmetbekov et al. (2010) 1 and Dulin et al. (2011) 5).

ACKNOWLEDGEMENTS

The work was partially supported by RFBR (grant N 10-08-01304-a) and Government of the Russian Federation (grant N 11.G34.31.0046, leading scientist – K. Hanjalic, Novosibirsk State University).

REFERENCES

1. Akhmetbekov Ye.K. et al. *Planar fluorescence for round bubble imaging and its application for the study of an axisymmetric two-phase jet.* Exp. Fluids. 2010, **48** (4), p. 615
2. Brandner P.A. et al. *An experimental investigation of cloud cavitation about a sphere.* J. Fluid Mech. 2010, **656**, p. 147
3. Cervone A. et al. *Thermal cavitation experiments on a NACA 0015 hydrofoil.* J. Fluids Eng. 2006, **128**, p. 326
4. Callenaere M. et al. *The cavitation instability induced by the development of a re-entrant jet.* J. Fluid Mech. 2001, **444**, p. 223
5. Dulin V.M. et al. *The optical principles of PFBI approach. Proc. of ISMTMF-7*, Tianjin, China, 2011, p. 217
6. Franc J.P. and Michel J.M. *Attached cavitation and the boundary layer: experimental investigation and numerical treatment.* J. Fluid Mech. 1985, **154**, p. 63
7. George D.L. et al. *Measurement of the bubbly flow beneath partial attached cavities using electrical impedance probes.* J. Fluids Eng. 2000, **122**, p. 151
8. Kawanami Y. et al. *Mechanism and control of cloud cavitation.* J. Fluids Eng. 1997, **119**, p. 788
9. Kubota A. et al. *Unsteady structure measurement of cloud cavitation on a foil section using conditional sampling technique.* J. Fluids Eng. 1989, **111**, p. 204
10. Laberteaux K.R. and Ceccio S.L. *Partial cavity flows. Part 1. Cavities forming on models without spanwise variation.* J. Fluid Mech. 2001, **431**, p. 1